https://doi.org/10.3311/PPme.46017
Creative Commons Attribution

Periodica Polytechnica Mechanical Engineering

Influence of Structural Vibrations on Polygonization on Tramways

Esther Moock[1*], Martin Rakowitsch[1], Raphael Pfaff[1]

[1] Chair and Institute for Rail Vehicles, RWTH Aachen University, Seffenter Weg 8, 52074 Aachen, Germany
[*] Corresponding author, e-mail: esther.moock@ifs.rwth-aachen.de

Received: 14 August 2026, Accepted: 02 October 2026, Published online: 03 November 2026

Abstract

Polygonization is one type of periodic wheel out-of-roundness that can diminish riding comfort and generate rolling and impact noises. Additionally, it may lead to the failure of various components, resulting in increased costs and compromising driving safety. Polygonization has been observed in several train operations. One proposed cause is the excitation of structural vibrations within the wheelset, which was, for example, observed when navigating tight curves. The objective of this paper is to enhance the understanding of the relationship between structural vibrations and the development of polygonization. To achieve this, a tram model with flexible wheelsets is established and simulated under tight curves with varying errors. A suitable wear model is implemented to assess wear across different scenarios. Ultimately, the correlation between worn wheels and structural vibrations is analyzed. A relationship between structural vibrations and the development of wheel polygonization could not be established. When negotiating tight curves, low velocities must be maintained due to limited lateral acceleration. With respect to the rather high frequencies of the examined structural modes, high polygon orders would be expected due to the relationship between the velocity, polygon order, and frequency. It was observed that factors such as constant curvature, an initial polygon shape, or rail corrugation play significant roles for polygon development.

Keywords

railway wheel polygonization, wheelset flexibility, tramways

1 Introduction

Polygonization is a periodic wheel out-of-roundness (OOR) resulting from non-uniform tread wear or initial OOR. Multiple wavelengths corresponding to different polygon orders may occur simultaneously along the wheel circumference. Polygonized wheels excite vibrations that lead to rolling noise, increased wear, and ultimately the failure of various components. As trams frequently operate in urban environments, the reduction of noise is of particular importance [1]. Depending on the type of operation, different polygon orders may develop while others are suppressed [2]. While wheel polygonization in high-speed trains has been extensively investigated, tram operation has received comparatively limited attention, despite significant differences in operating conditions and vehicle configurations. Trams frequently negotiate relatively tight curves, where increased wear is expected. Consequently, an investigation of polygon development under tram operating conditions is necessary.

The formation mechanisms of wheel polygonization have been examined by several researchers. Most explanations attribute its development to initial polygons introduced during wheel profiling and reprofiling or to wear-induced mechanisms. Wear-induced polygons may develop due to the excitation of fixed frequencies associated with the vehicle-track system, self-excitation, or resonance vibrations related to the eigenmodes of the wheelset. [3, 4] Previous studies have examined the relationship between the bending eigenfrequencies of the wheelset and the resulting polygon order, primarily focusing on high-speed vehicles, locomotives, and metros [5–8]. In the context of resonance-induced mechanisms, it has been shown that lateral slip associated with the first bending mode of the wheelset can contribute to polygon formation [7]. The torsion mode of the wheelset primarily induces longitudinal slip. However, in tram applications, independent wheelsets are commonly used, meaning that a torsional excitation does not occur.

The aim of this paper is to examine the relationship of the structural modes of a wheelset and polygon development in tram operation. It is structured as follows. First, an elastic

Cite this article as: Moock, E., Rakowitsch, M., Pfaff, R. "Influence of Structural Vibrations on Polygonization on Tramways", Periodica Polytechnica Mechanical Engineering, 2026. https://doi.org/10.3311/PPme.46017

wheelset model is implemented and integrated into a tram vehicle model. It is notable that the tram model uses normal wheelsets and not independent wheelsets. Subsequently, test tracks and corresponding irregularities are generated to investigate various operating scenarios. An iterative wear simulation is then performed and evaluated for each scenario. Finally, the structural modes, wheel/rail contact forces, and wear characteristics are analyzed to identify potential correlation among these factors.

2 Simulation set up

The simulation setup can be divided into three parts: the multibody simulation (MBS) model, the applied irregularities, and the wear calculation.

2.1 MBS model

For the simulation, a MBS model of a tram vehicle was developed using SIMPACK [9]. Fig. 1 illustrates the model of the wheelset and the vehicle, highlighting their respective degrees of freedom. The vehicle model comprises three components interconnected through force elements and rigid joints.

For the initial vehicle model a Flexity 2 consisting of five parts based on publicly available data and estimations, was employed. To optimize computational efficiency, the model was subsequently simplified to three parts and reduced by the rear bogie. The wheelset is composed of an elastic wheelset axle and two rigid wheels, which are elastically coupled to the axle. The axle is modeled as a finite element model with one-dimensional discretization, utilizing an Euler-Bernoulli beam approach. The elastic connection between the wheels and axle is implemented via a spring-damper model, facilitating lateral motion. Each wheel possesses one degree of freedom in lateral direction to capture the umbrella frequency under investigation. The design of the spring-damper-model ensures that the umbrella eigenfrequency is in a reasonable range. For the eigenmode analysis, both the first and second bending modes, as well as the torsion mode and umbrella mode, are examined. Fig. 2 presents these eigenmodes visually. A sampling frequency of 1000 Hz is utilized for time integration in accordance with Nyquist criteria to ensure accurate representation of dynamic behavior.

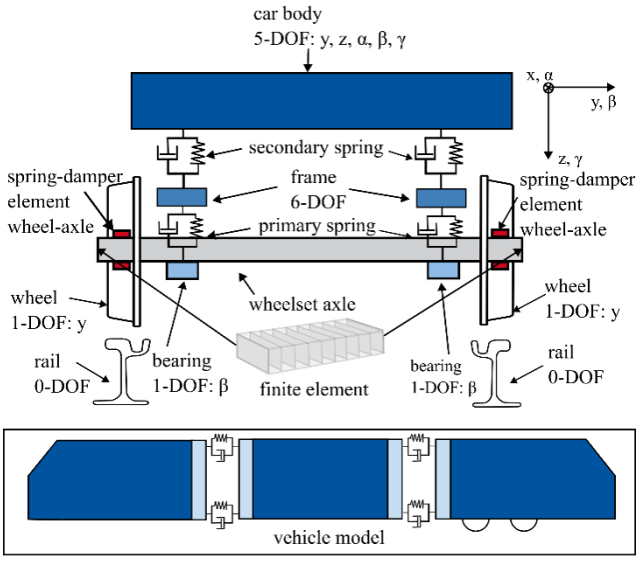
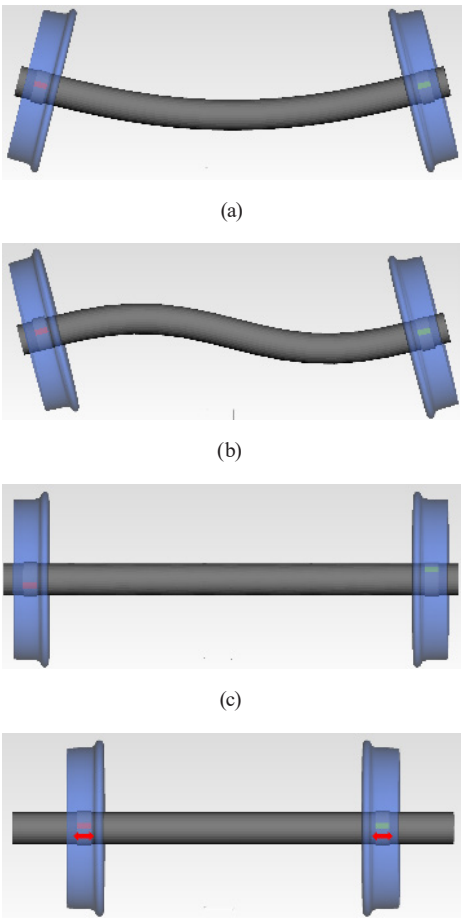


Fig. 1 Wheelset and vehicle model

2.2 Test tracks and irregularities

Research conducted on metros in China has demonstrated that polygonization can be influenced by track characteristics. It is assumed that particularly tight curves may affect the development of polygonization. [4] Self-excited vibrations arise when navigating tight curves in tram operation [10]. In this study, two tracks with small radii are



(a)

(b)

(c)

(d)

Fig. 2 Eigenmodes of wheelset: (a) Bending frequency (97 Hz); (b) Bending frequency (253 Hz); (c) Torsional frequency (93 Hz); (d) Umbrella frequency (406 Hz)

utilized for analysis. The first test track is a reversing track loop with a constant radius of 20 m, while the second test track features an S-curve configuration comprising a right-hand curve, a straight track of 3 m, and then a left-hand curve, both having a radius of 20 m. Grooved rails (59R12) are employed due to the tram's operation in mixed traffic conditions. Additionally, two track irregularities are introduced to assess the differences compared to an ideal track scenario. The synthetic track irregularity is derived from power spectral density (PSD) implemented within the MBS software according to ERRI B176 standards. Considering the eigenmodes of the wheelset within the range f=[90 Hz, 420 Hz] and maintaining a constant velocity of v=3.6 m/s, an interval for distance-based frequency can be calculated as Ω=[150m^{-1}, 750 m^{-1}]. As per documentation guidelines, the synthetic track irregularity is applicable for frequencies where 0.04 m^{-1} < $\Omega \leq$ 0.333 m^{-1}. Consequently, for the first track irregularity (TI1), this recommended distance-based frequency interval is utilized with irregularities in both horizontal and vertical directions. The second track irregularity (TI2) combines elements from the first track irregularity along with rail corrugation effects. In tram operations, rail corrugation characterized by a wavelength of 40 mm and a wear depth of 0.06 mm over approximately 20 m can be formed in curves with a radius of 30 m [11]. Therefore, for the second track irregularity, a cosine function based on these values is applied to model corrugation effects, which are then integrated into the overall irregularity according to ERRI B176 standards. Fig. 3 illustrates the various irregularities examined in this study. The horizontal and vertical misalignment of TI1 is shown with respect to the two test tracks, the reversed track loop (rtl)

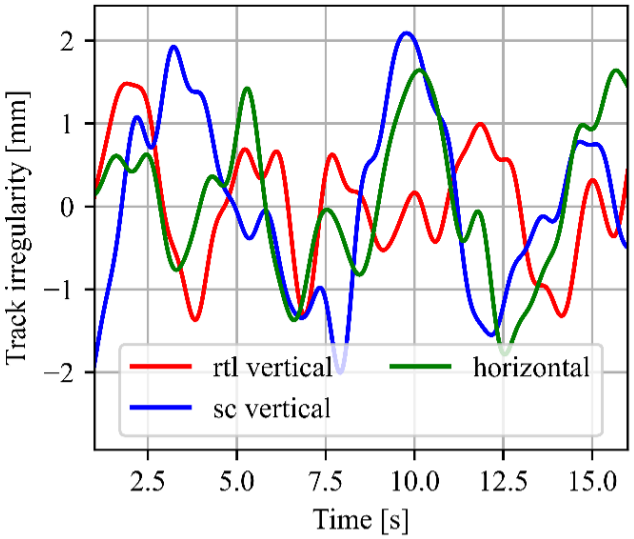


Fig. 3 Track irregularities without corrugation

and the S-curve (sc). For TI2, rail corrugation is added to TI1 in specific intervals, which is not included in Fig. 3. For the initial OOR, a 3rd order polygon is used with an initial wheel radius difference of 0.02 mm.

2.3 Wear calculation

Wear calculation can be approached through two distinct methods: local and global. In the local approach, the contact patch is discretized into infinitesimal elements, allowing for the calculation of the local wear distribution. Conversely, the global method utilizes wheel/rail forces to derive wear calculation. In this context, the FASTSIM algorithm, developed by Kalker [12], is employed to generate a local wear distribution based on MBS. Typically, these results are global and must be transformed into a localized framework. The wear model, according to Krause and Poll [13], is used and is based on the frictional power between wheel and rail. The excavated mass rate $\dot{m}$ is proportional to the wear energy P_R which is dissipated because of the friction in the wheel/rail contact. [5]

$$\dot{m} = \frac{k}{\rho} \times P_R \tag{1}$$

The frictional power P_R consists of three components that are dependent on the wheel/rail forces and relative velocities between the rail and wheel in longitudinal, lateral, and spin directions. [5]

$$P_R = T_x v_{rel,x} + T_y v_{rel,y} + M_B \Phi_{rel,b} \tag{2}$$

The wear coefficient

$$k\left[\frac{m^3}{Nm}\right]$$

is adopted from Krause and Poll [13] and is normally divided in two wear sections.

In the present work, three regimes are introduced in order to obtain a linear transition between mild and severe wear which is shown in Fig. 4 [14]. The density of steel, 7800 kg / m^3 is included in the definition of the wear coefficient. Since Krause and Poll [13] report a dependence of on relative humidity, a relative humidity of 80% is assumed here, and the wear coefficients are linearly interpolated with respect to humidity.

The excavated mass is computed for each time step around the wheel circumference over one wheel revolution. Wear is computed at each time step along the lateral profile to obtain the associated mass loss. This mass loss is subsequently applied uniformly to the wheel profile,

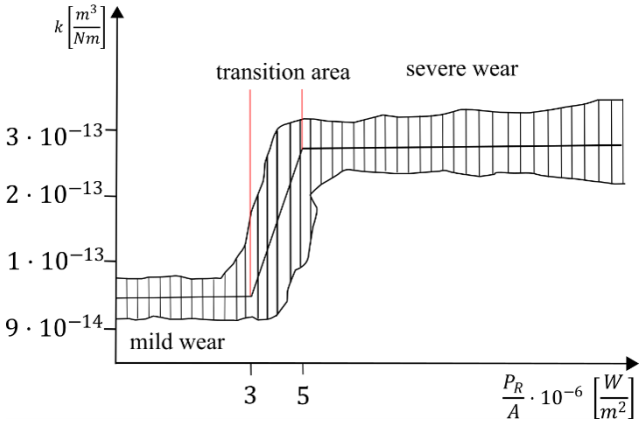


Fig. 4 Wear coefficient k over frictional power per area - similar to [14]

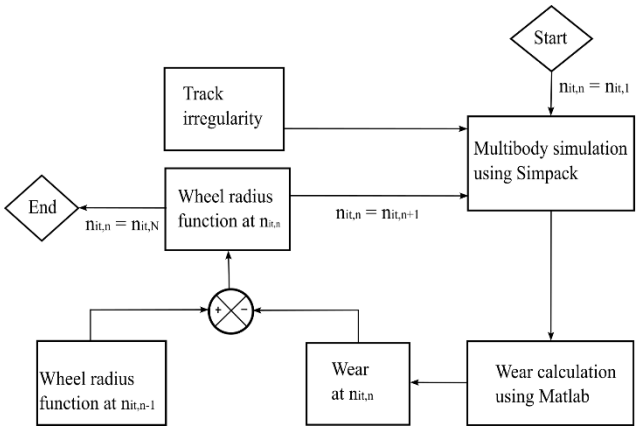


Fig. 6 Simulation process

such that the profile shape is preserved, whereas the wheel radius decreases over the course of the simulation. The change in radius Δr can be calculated as Eq. (3):

$$\Delta r(n) = \frac{k \times \left| T_x v_{rel,x} + T_y v_{rel,y} \right|}{A_n} \Delta t(n). \tag{3}$$

The spin moment is considered negligible.

For the time-discrete sampling, the contact patch is represented by an elliptical contact patch according to Hertzian contact theory. Given this time-discrete sampling, the wear depth along the circumference must be computed. The wear area of timestep n is modeled through two trapezoidal sections, as illustrated in Fig. 5.

The width of the contact area is defined at time steps, t_{n-1}, t_n and t_{n+1} The wear area of timestep n can thus be determined as A_n using Eq. (4):

$$A_n = l^- \times \left(\frac{b_n + (b_n + b_{n-1})/2}{2} \right) + l^+ \times \left(\frac{b_n + (b_n + b_{n+1})/2}{2} \right). \tag{4}$$

The length of the trapezoidal areas can be derived from the wheel radius and angular positions of the time steps. These lengths are defined as Eqs. (5) and (6):

$$l^- = \frac{1}{2} \times r \times (\vartheta_{n-1} - \vartheta_n), \tag{5}$$

$$l^+ = \frac{1}{2} \times r \times (\vartheta_n - \vartheta_{n+1}). \tag{6}$$

An iterative simulation process is employed to model polygonal wear evolution, as depicted in Fig. 6. Each current

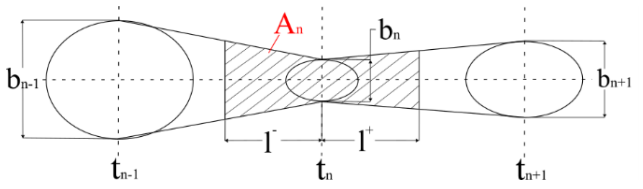


Fig. 5 Contact patch over time

iteration is indexed by $n_{it,n}$. For the initial iteration step, an initial wheel radius function and a track irregularity dependent on the scenario are applied. Wear calculations are performed based on contact forces and creepages obtained from the MBS results. The wear from one iteration is subsequently subtracted from the initial wheel radius function, yielding an updated wheel radius function that serves as input for the next iteration step. The initial OOR condition is defined within SIMPACK [9], where Fourier coefficients are utilized to update the OOR characteristics.

Due to the short simulation time of one iteration, a low-pass filter is applied to smooth cumulative wear across iterations. A Butterworth filter with a cutoff order of 50 has been selected. Finally, cumulative wear for each iteration step is scaled using Eq. (7):

$$w_{sf} = \frac{s_{tot}}{2\pi r \times n_i \times n_{r,con}}. \tag{7}$$

Here, s_{tot} represents a total test track length of 130 km, based on an assumption of passing the test track twelve times a day over six months before requiring reprofiling of wheels. The scaling factor also depends on the initial wheel radius r, which is assumed to be constant for this factor at 0.3 m. The number of iterations is denoted by n_i, while $n_{r,con}$ indicates the amount of wheel revolutions for each iteration step. In total, 20 simulation tests were conducted incorporating various test tracks, errors, and iteration steps.

3 Results

In the following, the results are presented to provide an insight into whether structural vibrations are excited under different scenarios and how they influence the development of polygon orders. The evaluation focuses on the reversing track loop with 25 iterations. For this analysis, the front left wheel is examined as a representative example

of wheel wear. The evolution of the radius throughout the iteration steps, the radius after the final iteration, a comparison of all four wheels on the bogie, and the developed Fourier coefficients are analyzed. For the comparison, the wheels are considered separately as front left (FL), front right (FR), rear left (RL), and rear right (RR). In scenarios involving TI1 and those without any irregularity, both profiles exhibit similarities, as illustrated in Fig. 7.

Each scenario develops a 1st order polygon with a polygon amplitude of 4 μm, resulting in approximately 0.1 mm of material removal per iteration. The front left wheel experiences the highest wear due to elevated wheel/rail forces while navigating curves. The second highest wear is ultimately observed on the inner rear wheel. With an initial OOR, the initial polygon remains rather unchanged. The 3rd order dominates the development of the polygon. However, eccentricity is also noticeable. The excavated mass during one iteration is comparable across both error types, with the front left wheel again exhibiting the most extensive wear. In contrast, TI2 demonstrates an increase in periodic irregularities throughout the iteration steps, which may be attributed to rail corrugation effects. The radius evolution and the radius after the full test track length for TI2 can be seen in Fig. 8.

When examining all four wheels of the bogie, differences in polygon orders emerge based on each wheel's position. Fig. 9 displays the Fourier coefficients for each wheel.

For the front left wheel, no predominant polygon order develops. While the front right wheel primarily exhibits lower polygon orders, a trend that is also evident in both rear wheels. Notably, the rear left wheel evolves a polygon of 48th order. For the rear right wheel low orders, 24th and 48th polygon orders develop.

Next, the wheel/rail forces are presented in Fig. 10, focusing on the lateral and longitudinal adhesion forces for the front left wheel across the four different error scenarios. Additionally, the amplitude spectrum is analyzed to provide further insights. Overall, it can be observed

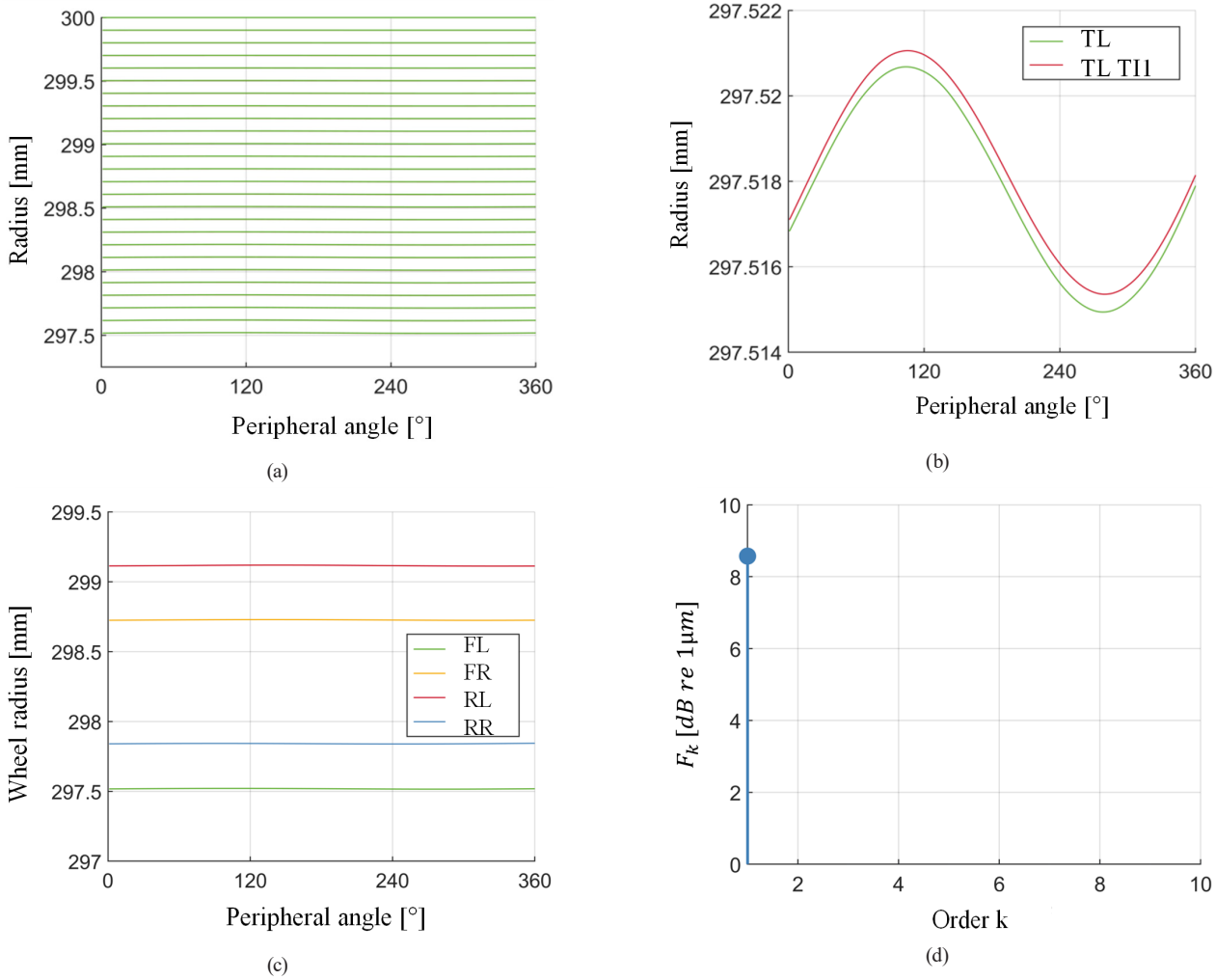


Fig. 7 Reversing track loop TI1/without error: (a) Radius evolution; (b) Radius after 25th Iteration; (c) Wheel comparison; (d) Fourier coefficient

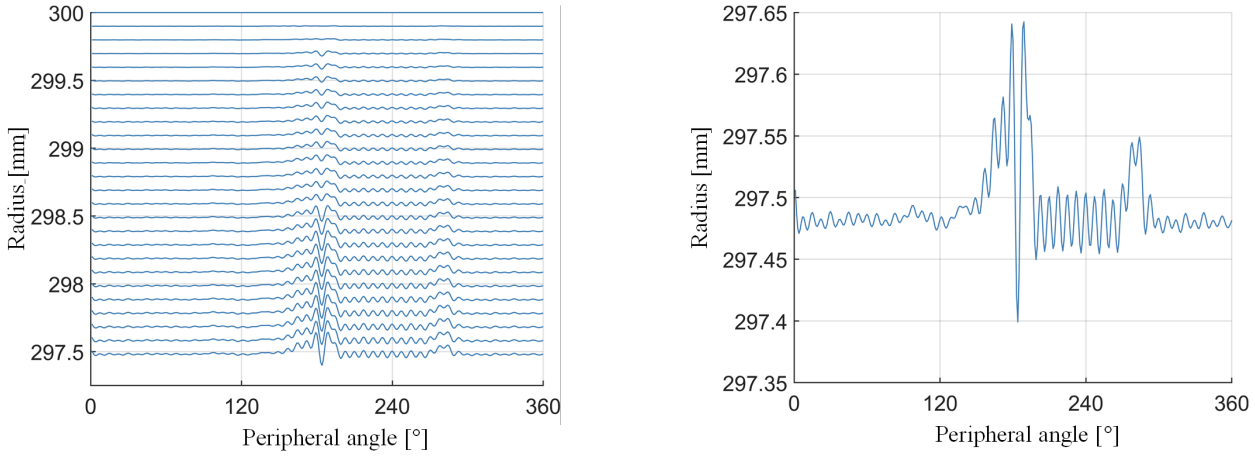


Fig. 8 Reversed track loop TI2: (a) Radius evolution; (b) Radius after 25th Iteration

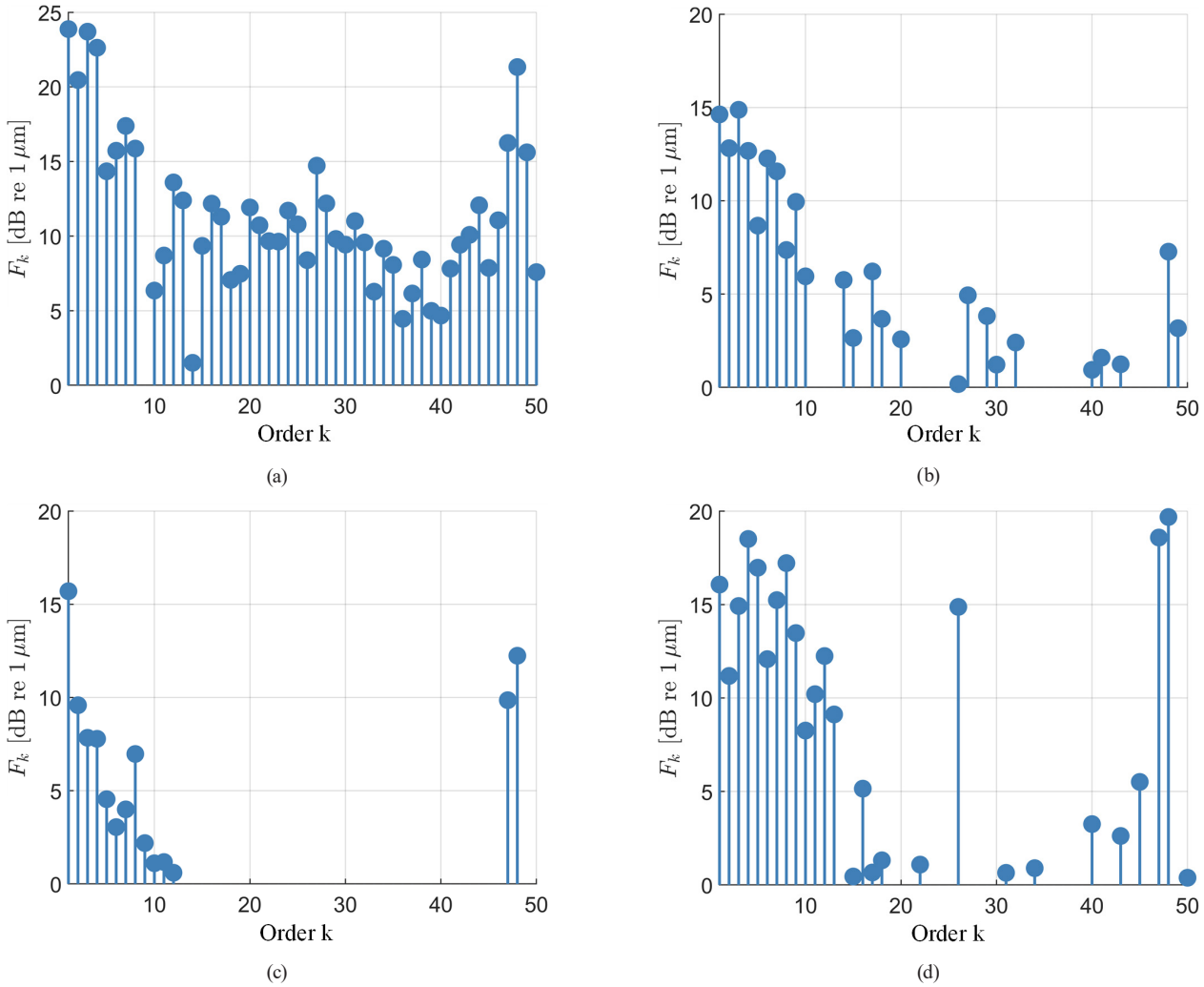


Fig. 9 Fourier coefficients TI2: (a) Front left; (b) Front right; (c) Rear left; (d) Rear right

that the behavior of both lateral and longitudinal adhesion forces is rather similar. In scenarios without an initial error, an oscillation with 2 Hz can be observed. However, when an initial OOR is introduced, this oscillation becomes superimposed with a 3rd order polygon. The relationship between frequency f, polygon order i, and velocity v is expressed by equation:

$$f = \frac{v}{\lambda} = \frac{v \times i}{2\pi r}. \tag{8}$$

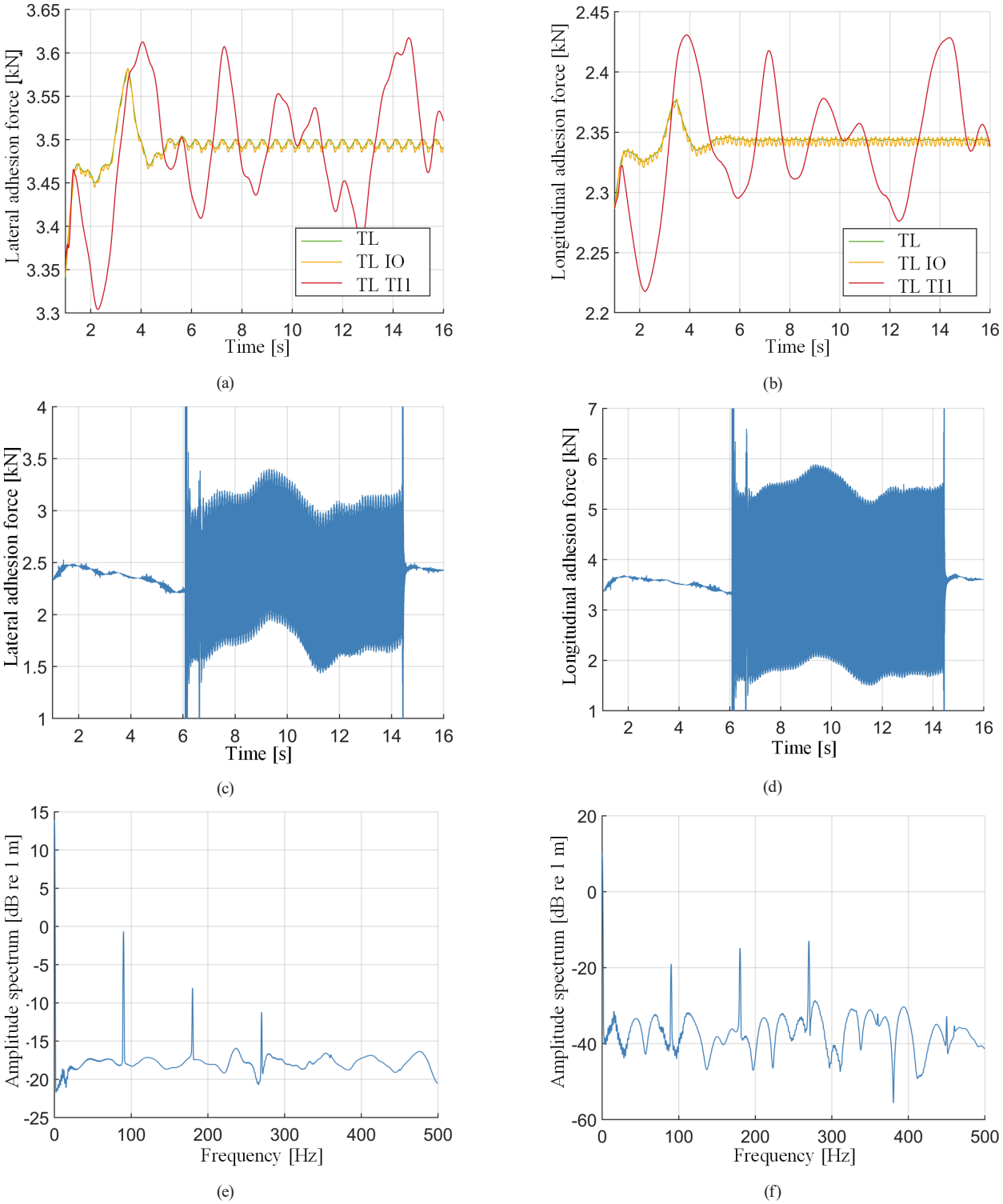


Fig. 10 Wheel/Rail contact forces: (a) Lateral adhesion force; (b) Long. adhesion force; (c) Lateral adhesion force TI2; (d) Long. adhesion force TI2; (e) Amplitude spectrum Tx TI2; (f) Amplitude spectrum Ty TI2

In cases involving TI1, the adhesion forces do not exhibit oscillations at a constant frequency. The wheel/rail forces show a pattern that is opposite to the pattern of the vertical track irregularities, which are shown in Fig. 3. The amplitude spectra for both adhesion forces appear quite similar.

High frequencies are not notably excited. For the reversing track loop with TI2, a contrast emerges in the interval where rail corrugation is present. This rail corrugation induces high-frequency oscillations with a high amplitude. The amplitude spectrum reveals that primarily excited frequencies occur at 90, 180, and 240 Hz. Using the aforementioned

equation, it can be established that the frequency of 90 Hz corresponds to the rail corrugation frequency. Thus, the other frequencies represent harmonics of this fundamental frequency. Regarding adhesion forces, differences in amplitude spectra are evident. For lateral adhesion force, primary excitation occurs at the rail corrugation frequency, whereas for longitudinal adhesion force, peak values are identified at the second harmonic corresponding to 240 Hz.

Further, structural modes are examined through specific parameters implemented for evaluation purposes. For the bending mode analysis, parameter is defined as the mean value between the left and right nodes at each end of the axle subtracted from the value of the middle node in vertical direction. Fig. 11 (a) and (b) illustrate this bending mode over time for each error scenario. A consistent excitation at 2 Hz is observable across nearly all errors. However, when rail corrugation is applied, an increase in amplitude becomes apparent with predominant excitation at corrugation frequency. Fig. 11 (c) and (d) show both the amplitude spectrum and the corresponding frequency spectrum for TI2 on the reversing track loop.

The amplitude spectrum indicates dominant peaks corresponding to the corrugation frequency along with their harmonics while showing no distinct peaks associated with bending mode frequencies. In the spectrogram it is shown that lower frequencies are excited throughout the total test track, while higher frequencies become prominent when traversing areas affected by rail corrugation.

For the torsional mode, the rotation of the axle is examined. The parameter is defined as the difference between the rotation of the left node at the end of the wheelset axle and the rotation of the middle node. Fig. 12 shows that, in the reversing track loop without an error, an excitation at 2 Hz is observed. This is superimposed by the polygon frequency when an initial OOR is present. For TI1, a mirrored progression of the wheel/rail forces is noted. When rail corrugation is introduced, the corrugation frequency dominates again, with its harmonics also being excited. Although the

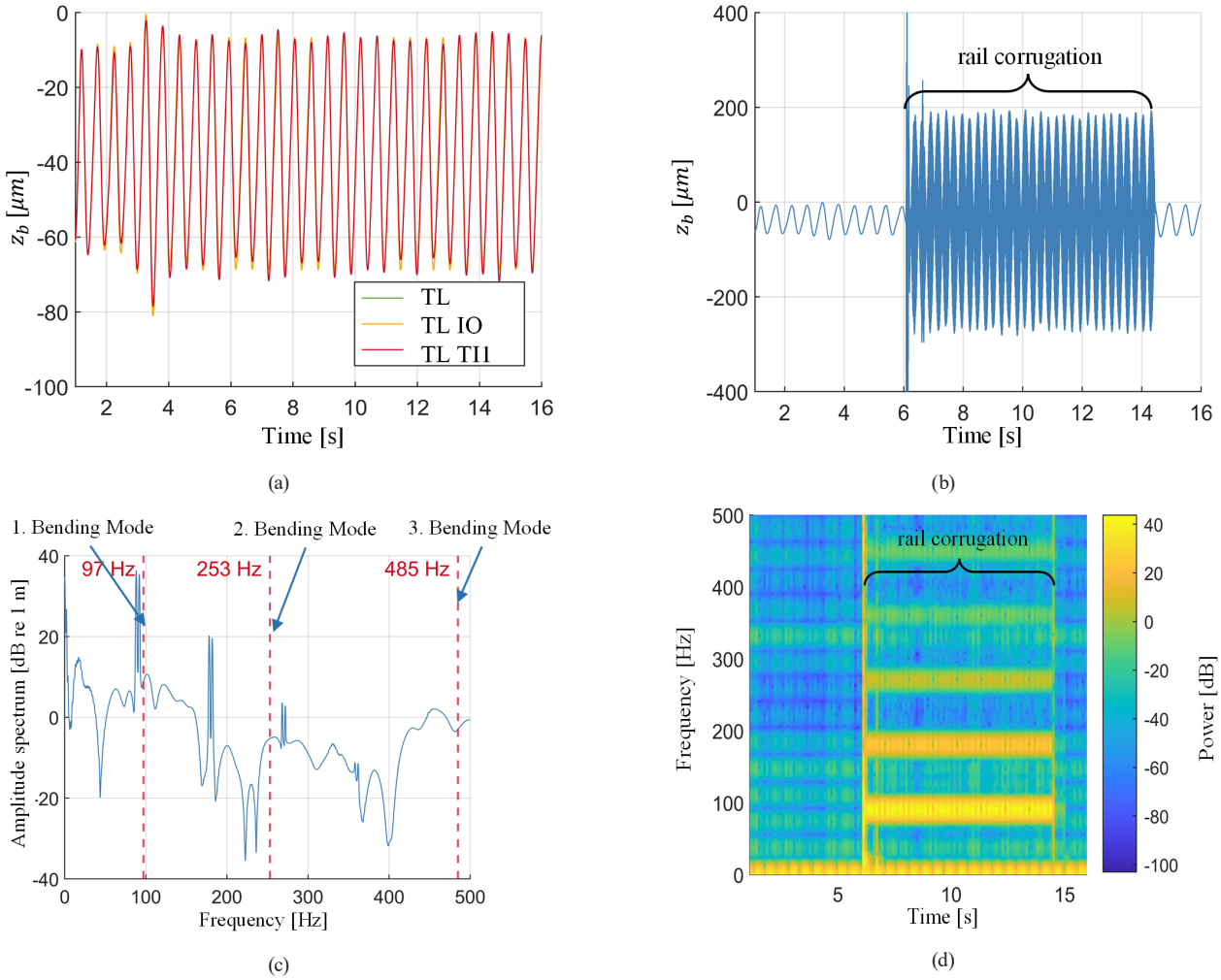


Fig. 11 Bending mode: (a) Parameter z_b; (b) Parameter z_b TI2; (c) Amplitude spectrum TI2; (d) Spectrogram TI2

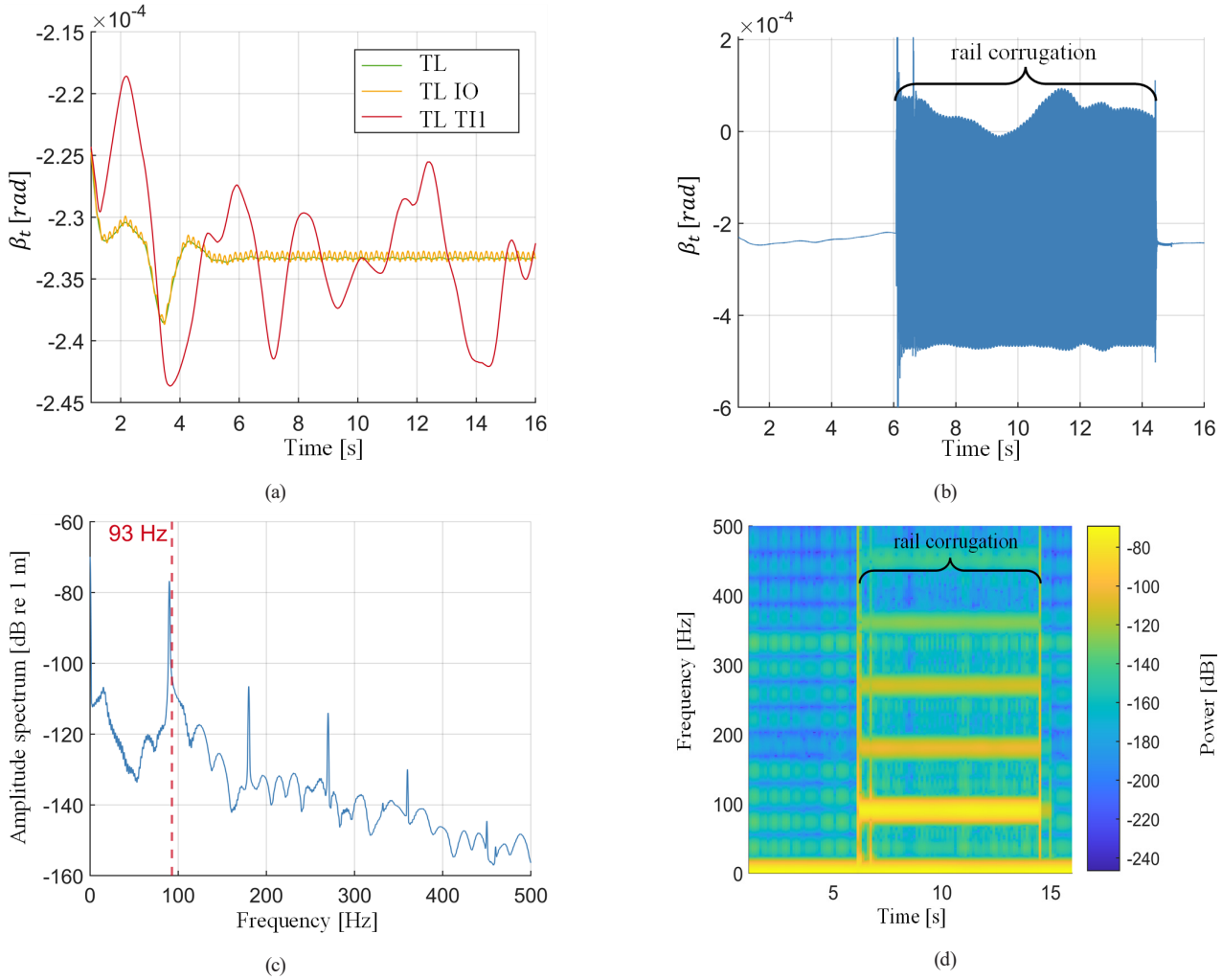


Fig. 12 Torsional mode: (a) Parameter β_t; (b) Parameter β_t; (c) Amplitude spectrum TI2; (d) Spectrogram TI2

torsion frequency of 93 Hz is very close to the corrugation frequency, it does not exhibit significant excitation.

Lastly, the umbrella mode is examined as the parameter defined by subtracting the middle and left nodes of the wheelset axle in the lateral direction. The umbrella mode for the different error scenarios is presented in Fig. 13. Similar to observations made for the torsional mode, an excitation at 2 Hz occurs in a reversing track loop without errors. In the scenario involving initial OOR, the signal becomes superimposed with the polygon frequency. Regarding TI1, there are no consistent oscillations. However, similarities to responses observed at the onset of the torsional mode are evident.

TI2 exhibits pronounced peaks at both the beginning and end of the corrugation interval due to its implementation using a cosine function. Within this interval, primarily the corrugation frequency of 90 Hz and the first harmonic with 180 Hz are excited across frequencies up to 200 Hz. An increase around 410 Hz is also observed, which aligns closely with the umbrella frequency at 406 Hz. However, it cannot be definitively concluded that the umbrella mode is stimulated.

Overall, the results show that, in the absence of errors, a low-frequency excitation at 2 Hz occurs during constant-radius curve running. Since the wheel/rail forces in TI1 primarily follow the profile of the track irregularity, yet an almost identical wheel profile develops without track irregularities, it is concluded that the predominantly long-wave track irregularity has no significant impact on wear development. With an initial OOR applied, the initial polygon remains unchanged. Regarding structural vibrations, the polygon frequency influences only the torsional and umbrella modes, as the constant oscillation at 2 Hz is superimposed by the polygon frequency. With TI2, wear behavior is predominantly governed by rail corrugations. The corrugation excites primarily the corrugation frequency of 90 Hz and its respective harmonics resulting from constant speed. The bending and torsional modes of the wheelset axle are not demonstrably excited, although increased excitation around the umbrella frequency is

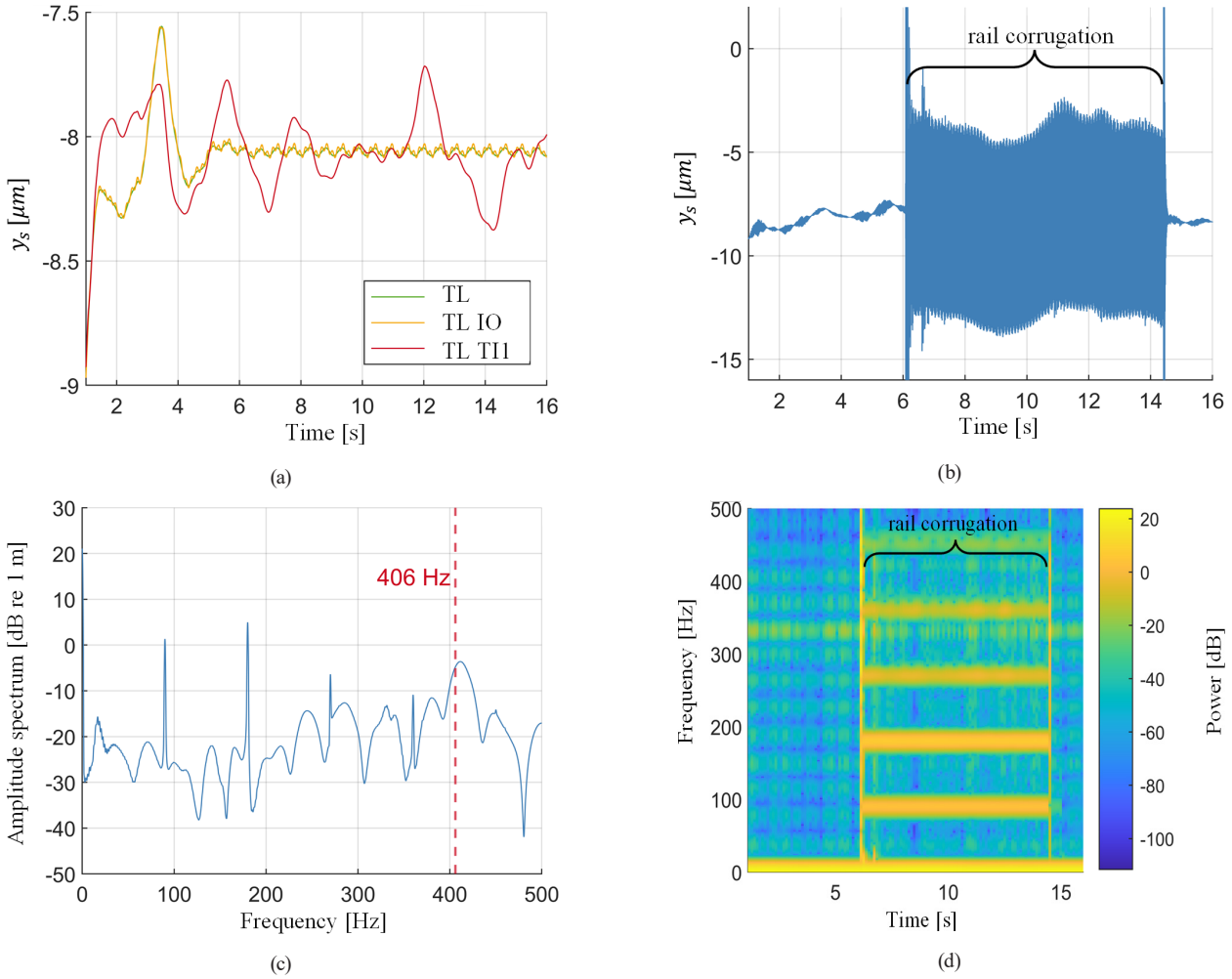


Fig. 13 Umbrella mode: (a) Parameter y_s; (b) Parameter y_s TI2; (c) Amplitude spectrum TI2; (d) Spectrogram TI2

observable. In terms of radius development, particularly higher-order polygons are prominent. The distribution of polygon orders specifically exhibits 1st and 48th order polygons. The 48th order can be attributed to their correlation with the 90 Hz.

In summary, it has been shown that wheelset eigenmodes could not be demonstrably excited by applying initial errors. Various test tracks were selected to create different conditions under which wheelset eigenforms could potentially be excited. However, it has become evident that polygon formation arises primarily from track irregularities or alignment issues. During constant curve travel, a 1st order polygon with low amplitude forms, but the wear pattern is changed with respect to the s-curve so that no polygon is formed. Track irregularities only influence wear development when they possess wavelengths exceeding those associated with the first polygon frequency. It is therefore assumed that only wavelengths below 1.88 m may have an impact on polygon formation.

Referring to Eq. (8), one would expect very high polygon orders to arise from the excitation of the eigenforms of the wheelset because of a relatively low velocity. This expectation is reflected in Table 1. The expected polygon orders above 50 were not covered within the examined range. Furthermore, it raises questions about whether such high orders fulfill the definition of a polygon wear pattern. Ultimately, it can be argued that wheelset eigenfrequencies may influence polygon formation more prominently in high-speed operations than in tram operations since higher speeds would lead to significantly lower polygon orders being generated.

Table 1 Polygon orders of Wheelset Eigenmodes

Eigenmode	Frequency [Hz]	Polygon order
1st Bending mode	97.3	51
2nd Bending mode	252.6	132
Torsional mode	93.2	49
Umbrella mode	406.3	213

4 Conclusions

This paper investigates the relationship between structural vibrations of wheelsets and polygon formation during tight curve navigation in tram systems. Initially, it was essential to determine whether the structural vibrations of the flexible wheelset are excited in curved tracks. To achieve this, a flexible wheelset model was developed and integrated into a vehicle model. Subsequently, this model was simulated under various error types on tight curves. The iterative wear was calculated for different scenarios, and an analysis was conducted to explore the correlation between wheel/rail forces, wheelset profiles, and polygon formation.

The results indicated that the structural vibrations of the wheelset were not demonstrably excited. Therefore, no direct connection could be established between these vibrations and the development of polygonal wheels. Although polygonal wheels did emerge in some scenarios, they were primarily attributed to constant curve navigation, initial polygons, or rail corrugation in TI2. Additionally, due to the low speeds associated with tight curve navigation, very high polygon orders would be expected if they were to correlate with the eigenforms of the wheelset. Consequently, it is proposed that the eigenmodes of the wheelset likely exert a more significant influence on polygon formation at higher speeds.

Further research could utilize field measurements compared against simulations. A vehicle model known to experience polygon formation in actual operation should be employed for such studies. Moreover, investigations involving vehicles operating at higher speeds could be conducted to examine whether excitation of structural vibrations promotes polygon formation under those conditions.

References

[1] Staśkiewicz, T., Firlik, B. "Out-of-round tram wheels – current state and measurements", Archives of Transport, 45(1), pp. 93–103, 2018. https://doi.org/10.5604/01.3001.0012.0946

[2] Tao, G., Wen, Z., Guan, Q., Zhao, X., Luo, Y., Jin, X. "Locomotive wheel wear simulation in complex environment of wheel-rail interface", Wear, 430–431, pp. 214–221, 2019. https://doi.org/10.1016/j.wear.2019.05.012

[3] Johansson, A., Andersson, C. "Out-of-round railway wheels—a study of wheel polygonalization through simulation of three-dimensional wheel–rail interaction and wear", Vehicle System Dynamics, 43(8), pp. 539–559, 2005. https://doi.org/10.1080/00423110500184649

[4] Iwnicki, S., Nielsen, J. C. O., Tao, G. "Out-of-round railway wheels and polygonisation", Vehicle System Dynamics, 61(7), pp. 1787–1830, 2023. https://doi.org/10.1080/00423114.2023.2194544

[5] Fu, B., Bruni, S., Luo, S. "Study on wheel polygonization of a metro vehicle based on polygonal wear simulation", Wear, 438–439, 203071, 2019. https://doi.org/10.1016/j.wear.2019.203071

[6] Peng, B., Iwnicki, S., Shackleton, P., Crosbee, D., Zhao, Y. "The influence of wheelset flexibility on polygonal wear of locomotive wheels", Wear, 432–433, 102917, 2019. https://doi.org/10.1016/j.wear.2019.05.032

[7] Morys, B. "Enlargement of Out-of-Round Wheel Profiles on High Speed Trains", Journal of Sound and Vibration, 227(5), pp. 965–978, 1999. https://doi.org/10.1006/jsvi.1999.2055

[8] Tao, G., Wang, L., Wen, Z., Guan, Q., Jin, X. "Experimental investigation into the mechanism of the polygonal wear of electric locomotive wheels", Vehicle System Dynamics, 56(6), pp. 883–899, 2018. https://doi.org/10.1080/00423114.2017.1399210

[9] Dassault Systèmes "Simpack, (2025)", [computer program] Available at: https://www.3ds.com/de/produkte-und-services/simulia/produkte/simpack/ [Accessed: 16. 03. 2025]

[10] Zehetbauer, F., Edelmann, J., Plöchl, M. "A minimal model to study self-excited vibrations of a tram wheelset in curves with small radius of curvature", Vehicle System Dynamics, 61(11), pp. 2867–2887, 2023. https://doi.org/10.1080/00423114.2022.2139728

[11] Wang, Z., Lei, Z., Zhu, J. "Formation Mechanism of Rail Corrugation for Modern Tram Lines", Periodica Polytechnica Civil Engineering, 68(3), pp. 987–998, 2024. https://doi.org/10.3311/PPci.24748

[12] Kalker, J. J. "Wheel-rail rolling contact theory", Wear, 144(1), pp. 243–261, 1991. https://doi.org/10.1016/0043-1648(91)90018-P

[13] Krause, H., Poll, G. "Wear of wheel-rail surfaces", Wear, 113(1), pp. 103–122, 1986. https://doi.org/10.1016/0043-1648(86)90060-8

[14] Meinders, T., Meinke, P. "Rotor Dynamics and Irregular Wear of Elastic Wheelsets", In: System Dynamics and Long-Term Behaviour of Railway Vehicles, Track and Subgrade, Springer, 2003, pp. 133–152. ISBN 978-3-540-45476-2 https://doi.org/10.1007/978-3-540-45476-2_9